Precipitation over concave terrain

Qingfang Jiang, UCAR visiting scientist
Naval Research Laboratory, Monterey, CA

1. INTRODUCTION

The motivation of this model-based idealized study can be illustrated using Fig 1. Apparently, according to the long-term climatology, precipitation over the Alpine area tends to be oriented along the Alps. The southern side of the Alps is wetter, likely associated with warm moist air from the Mediterranean. However, the precipitation is not uniform at all. There are 'wet spots' with precipitation twice as much as their neighboring areas; one is located over Lago Maggiore-Toce area and the other is located at the northeastern tip of Italy. It is especially interesting that both wet-spots are located upstream of the vertices of concave-terrain (indicated by red lines in Fig. 1) relative to the southerly flow. Between the two wet spots, there is a precipitation minimum, coincided with the vertex point (where two ridges intercept) of a convex-terrain shape. To some extent, complex terrain such as the Alps is composite of concave or convex terrain of different scales. For example, the main Alpine chain is concave relative to southerly wind and convex to northerly wind. The dynamical funneling effect of concave-terrain and its implication on precipitation enhancement is investigated in this study through a series of three-dimensional idealized simulations. The rest of the paper is organized as follows. In section 2, some modeling aspects and relevant control parameters and indices are introduced. The sensitivity of flow confluence and stratiform precipitation to a few parameters is examined in section 3. The nonlinear dynamics associated with stratiform precipitation is discussed in section 4. The results are summarized in section 5.

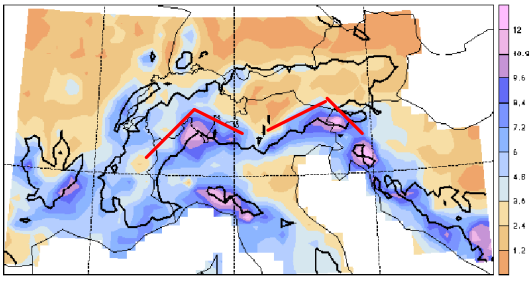

Figure 1. Mean precipitation (mm/day) over the Alpine area for October from 1971 to 1990 (see Frei and Schar 1998). The red lines indicate the location of the concave-terrain described in the text.

2. MODELING ASPECTS

2.1 COAMPS

The atmospheric component of the Coupled Ocean-Atmosphere Mesoscale Prediction System (COAMPS™) is used for this idealized study. COAMPS is a nonlinear, nonhydrostatic and compressible model featuring a terrain-following coordinate system and a suite of physical parameterizations (Hodur 1997). For simplicity, Kessler's warm rain scheme (Kessler 1969) is used and no ice-phase cloud physics is included in this study. The computational domain is defined by a grid of 151X151 points with a horizontal resolution of 5 km. The model top is at 20 km with 50 irregularly spaced vertical levels.

2.2 Idealized Terrain

The concave-terrain is idealized as a pair of mirror-symmetric ridges described by the following equations,

$$h(x,y) = \frac{h_m}{1 + x'^2/a^2 + y'^2/b^2}, \quad for\ |y| > b$$

$$= \frac{h_m}{1 + x'^2/a^2}\left(1 + b\cos(py/b)\right), \quad for\ |y| \le b \qquad (1)$$

where,

$$x' = x\cos a + (y-b)\sin a$$
$$y' = (y-b)\cos a - x\sin a \qquad (2)$$

for y>0, and

$$x' = x\cos a - (y+b)\sin a$$
$$y' = (y+b)\cos a + x\sin a \qquad (3)$$

for $y \le 0$. According to the above equations, the concave terrain is described by six parameters, namely, the ridge height h_m, ridge half width a, ridge length b, angle of concavity a, and gap parameter ß. The plane-views of the concave terrain for varying parameters are shown in Fig. 3.

* Corresponding author address: Qingfang Jiang, Naval Research Laboratory, Monterey, CA 93943-5502; email:Jiang@nrlmry.navy.mil

2.3 Idealized Sounding

The sounding used in this study is shown in Fig. 2. It was modified from the 1105UTC Milan sounding on 21 October 1999 observed during intensive observing period (IOP) 8 of the Mesoscale Alpine Programme (MAP; Bougeault et al. 2001). MAP IOP 8 was characterized by moderate stratiform precipitation over the southern Alps (Houze 2001). For the purpose of simplicity, the potential temperature and relative humidity profiles were smoothed, and the wind was replaced by a westerly wind with uniform wind speed U=15ms^{-1}. The environment flow specified by this modified sounding features a stable moist layer with a moist buoyancy frequency $\mathbf{N_m}$ around 0.01 s^{-1}.

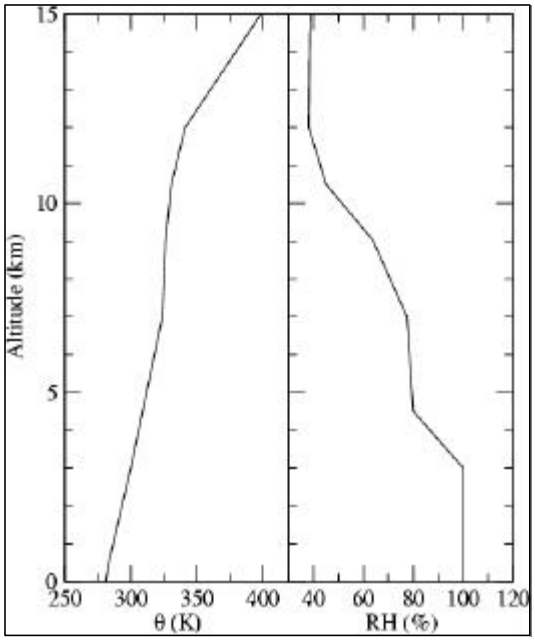

Figure 2. The profiles of potential temperature ? and relative humidity (RH) for the idealized sounding.

2.4 Relevant Parameters and Indices

Symbolically, a solution to the above setup can be written as

$$f(x, y, x, t) = f(x, y, z, t; \; U, N, rh, f, a, b, h_m, a, b) \quad (4)$$

where, U, N, and rh are the ambient windspeed, buoyancy frequency, and relative humidity in the lower troposphere specified by the idealized sounding, f is the rotation coefficient, and the rest are terrain-related parameters. In this study, unless specified otherwise, the following parameters are used for the simulations: a=15 km, b cos(a) =50km, h_m=1200m, a=30, ß=0.0, and f=0. With b cos(a) = constant, the vertical interception areas of the concave-terrain relative to the wind along the x-axis are independent of the concave angle a.

We are primarily interested in the dynamical response of the low-level moist flow over the windward side of the terrain. For the convenience of discussion, we define the following quantities or indices:
Nondimensional mountain height, $\mathbf{M=N_m h_m/U}$, where $\mathbf{N_m}$=0.01 s^{-1} is the moist buoyancy frequency.
Windward blocking index, $u_b = u_{min}/U$, where u_{min} is the minimum across-mountain wind at the surface.
Non-dimensional maximum vertical motion over the wind-slope, $\mathbf{w_m = 2 w_{max} a/Uh_m}$, where $\mathbf{w_{max}}$ is the maximum vertical motion over the windward side and below 2 km.
Non-dimensional maximum vertical motion at the surface, $\mathbf{w_{sm} = 2 w_{smax} a/Uh_m}$ where $\mathbf{w_{smax}}$ is the maximum vertical motion at the surface, which is associated with direct upslope lift.
Confluence, $C(x,y,z) = dv/dy$; Flow is confluent as C<0 and diffluent otherwise.
Stream-wise averaged precipitation rate (mm/h),

$$PR(y) = \int p(x, y)dx \Big/ 6a$$

where p(x,y) is the accumulated precipitation between t=10 and t=16 hours.
Scaled Integrated precipitation

$$Pt = \iint p(x, y)dxdy \Big/ 6ab$$

P_t has the unit of mm/h.

3. STRATIFORM PRECIPITATION

3.1 *Sensitivity to Concave Angle*

The effect of the terrain concave angle on upslope lift and precipitation can be illustrated by comparing the three solutions with a=0, 30, -30 respectively (see Figs. 3a, 3b and 3d). The vertical interception areas of the three terrain relative to the westerly wind are identical. As expected, precipitation over the straight ridge is quite uniformly distributed along the windward slope. Upstream of the ridge, the low-level flow is diffluent as it approaches the ridge. The diffluence zone extends approximately 150 km upstream. Flow confluence only exists near the two ends of the ridge. Clearly, relative to the straight ridge, precipitation over the concave-terrain is significantly enhanced over the triangle area upstream of the vertex of the concave-terrain. Comparing to the straight ridge run, the run simulations with concave-terrain show much reduced flow diffluence near the center streamline with a small confluence-zone located right upstream of the vertex.

The strength and area of the confluence-zone increases with increasing concave angle. Precipitation around the vertex increases accordingly. In contrast, for moist flow passes convex terrain, precipitation is weaker near the terrain-vertex and precipitation maxima are located approximately 40 km away from the centerline. Strong diffluence is present upstream of the vertex, which is consistent with the presence of the precipitation minimum. The cross-stream distribution of precipitation during t=10 and 16 hrs for a=-30,0,30,45 is shown in Fig. 4a. For concave-terrain, precipitation is significantly enhanced near the vertex. The enhancement tends to increase with the concave angle. For example, at Y=0, precipitation for a=45 is three times the value of that for a=0. For convex-terrain, precipitation maxima are located at Y=±30km and the precipitation at Y=0 is approximately 30% weaker than the maximum precipitation. Clearly, the flow patterns over the lee-side are quite sensitive to the concave angle as well, which is beyond the scope of this paper.

3.2 Sensitivity to Mountain Height

For a=30, and h_m =600, 1200, 1800m (i.e., Figs. 3c,3b, and 3f), the solutions indicate the presence of three distinctive regimes. For lower terrain, the solution features linear dynamics. Although, far upstream flow is still diffluent, there is a well-defined confluence-zone located upstream of the vertex which is approximately 30 km wide and 50 km long (Fig. 3c). Accordingly, precipitation upstream of the terrain vertex is significantly enhanced. As mountain increases, the solution moves into a nonlinear regime with blocking dominant and the confluence area upstream of the vertex becomes much smaller (Fig. 3a). In both the linear and nonlinear regimes, the precipitation maximum is located near the vertex. Further increasing the mountain height may cause flow reversal and recirculation over the windward slope, Although flow confluence is present associated with the flow reversal (Fig. 3e), with downward motion at the surface, the total vertical motion is relatively weak. The precipitation maxima are located near the two ends of the convex-terrain. Further upstream, there is a bow-shaped precipitation band which propagates against the mean flow at a speed of approximately 3.4 ms^{-1}. This precipitation band is associated with an upstream propagating nonlinear wave and it decays slowly with upstream distance due to wave dispersion. The cross-stream precipitation distribution for a=30 and a range of mountain height is shown in Fig. 4b. Clearly, for h_m =300, 600, 1200, 1500m, the precipitation maximum is located upstream of the concave-vertex, indicative of precipitation enhancement associated with flow confluence. For h_m =1800m and 2100m, precipitation near the vertex is the same or even weaker than that over neighboring ridges.

3.3 Sensitivity to Gap Parameter

The solution with a 400 m deep gap at the vertex of the concave-terrain (i.e., ß=-0.2) is shown in Fig. 3e. Clearly, associated with the strong flow confluence upstream of the vertex, the precipitation maximum is located upstream of the gap. There are two secondary precipitation maxima coincided with the higher peaks.

The cross-stream precipitation distribution for four simulations with ß=-0.3,-0.2,0.,0.2 is shown in Fig. 4c. Comparing with ß=0, precipitation for ß=-0.2 is significantly weaker near the vertex. As the gap becomes deeper, the precipitation maximum at the vertex only changes slightly. The precipitation distribution for ß=0.2 is similar to that for ß=0. However, further analysis indicates that the dynamics is quite different for the two simulations. The simulation with ß=0.2 shows stronger windward blocking, stronger diffluence, and low-level wind reversal. Accordingly, upstream of the vertex, the precipitation is weaker, but more widespread in streamwise direction.

3.4 Sensitivity to Other Parameters

In this study, the sensitivity of precipitation to the ridge width and earth rotation was investigated as well. Comparisons among three simulations with a=30, and h_m =1200m, and bcosa=30, 50, and 100 km indicate that while a longer ridge does help to increase the windward flow confluence, the value of the precipitation maximum shows little sensitivity to the ridge length. It should be noted that for the simulation with bcosa= 100 km, the boundary conditions were derived from a coarser grid mesh with ?x=15km to reduce the influence from the boundaries.

Simulations have been performed with $f=10^{-4}$ and $1.4x10^{-4}$ s^{-1} respectively to examine the impact of the earth rotation on flow funneling and precipitation. The ambient flow is in geo-strophic balance. With $U=15ms^{-1}$ and horizontal scale~2b~100km, we have the Rossby number Ro~1.5,1.0. Primary results indicate that the rotation tends to increase precipitation near the terrain vertex through increasing windward flow confluence.

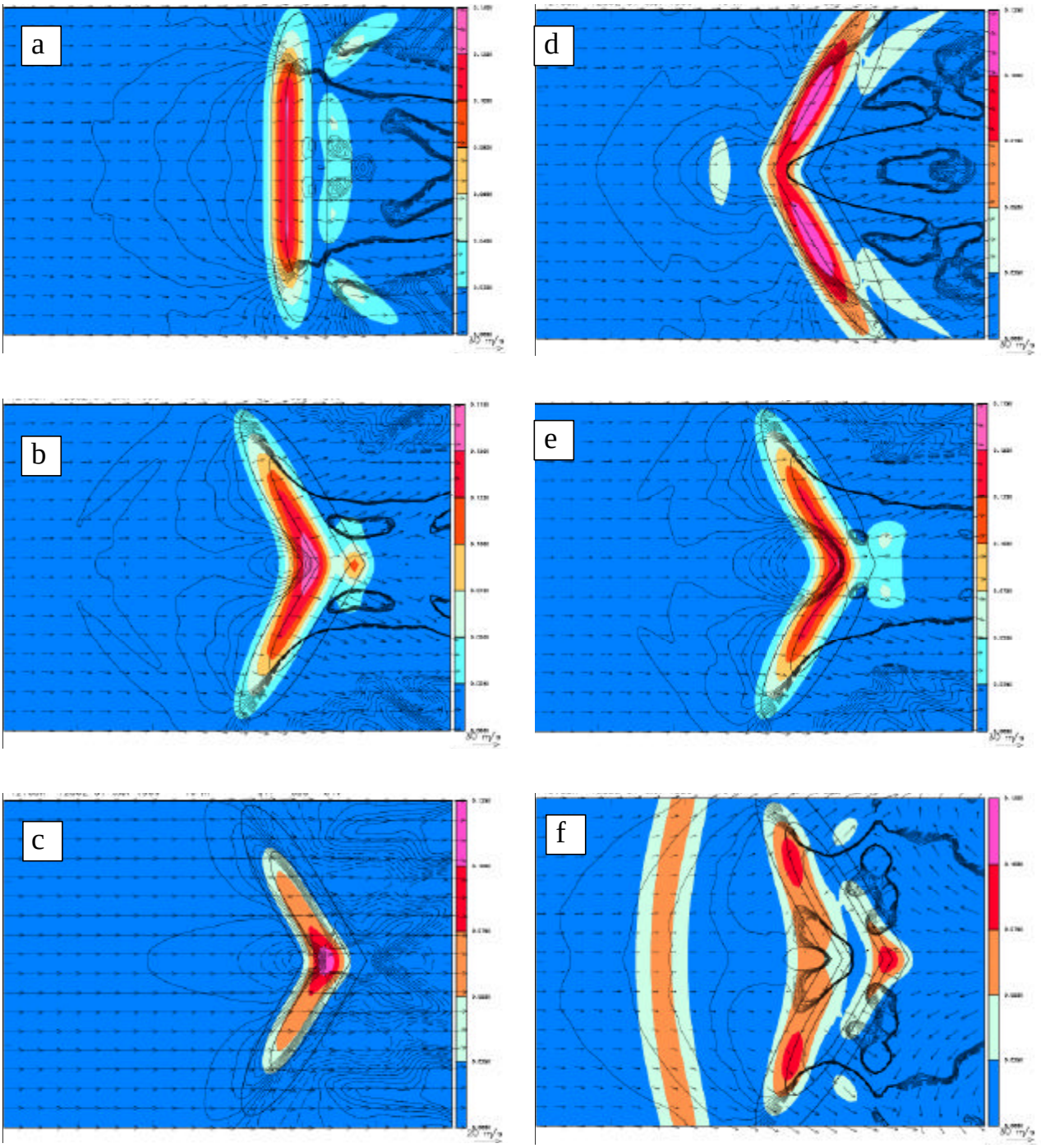

Figure 3. Horizontal wind vectors, rain-water mixing ratio (g/kg, in color), terrain (dark contour, increment=hm/3), and flow confluence (x10 $^{-5}$ s $^{-1}$, only values between –5 and 5 are contoured, increment=1, negative contours are dashed) at the surface and model time t=12 hour derived from six simulations with a=15km and b=50km, namely: a) a=0 and h_m=1200m; b) a=30 and h_m=1200m; c) a=30 and h_m =600m; d) a=-30 and h_m=1200m; e) a=30, h_m=1200m, and ß=-0.2; f) a=30 and h_m=1800m.

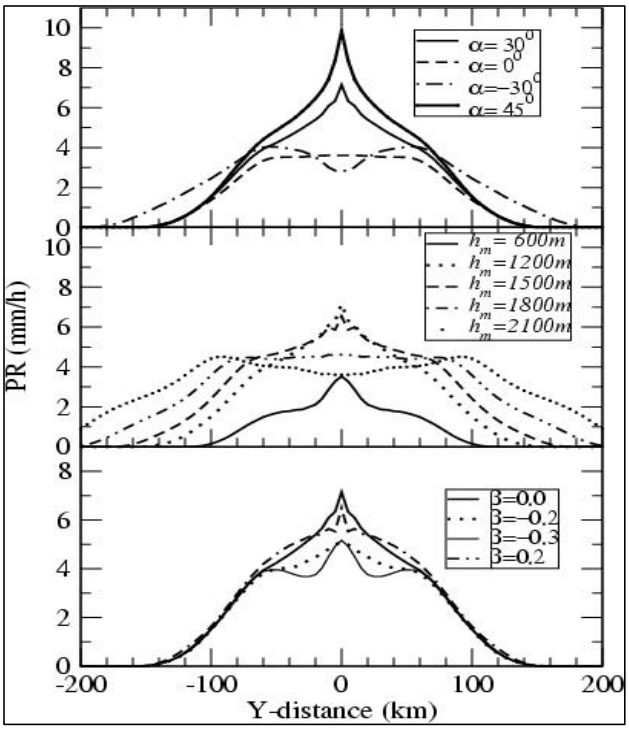

Figure 4. Plot of streamwisely averaged precipitation rate (mm/h) as a function of cross-stream distance.

4. FUNNELING and BLOCKING

Apparently, flow confluence or funneling occurred upstream of the concave-terrain is closely related to windward flow blocking.

The upslope lift which is the key element in orographic precipitation enhancement can be decomposed into two components, namely, direct upslope lift (DUL) and lift associated with low-level flow convergence (LFC). DUL is proportional to the product of U and the streamwise mountain slope and decreases with increasing altitude. LFC is proportional to flow convergence and increases with increasing altitude to the level where the divergence is zero. For low terrain DUL dominates and the strongest vertical motion is at the surface. As the terrain becomes higher, the decrease of u associated with blocking may overpower the increase of the mountain slope. As a result, flow convergence becomes more important and the vertical motion maximum is located above the ground. Convergence induced by windward blocking and its impact on precipitation has been examined by Jiang (2003).

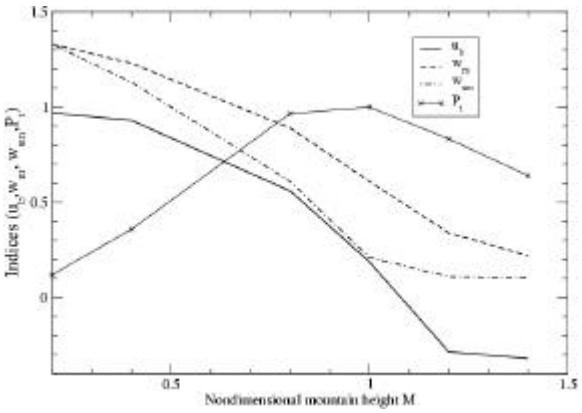

Figure 5. The plot of u_b, w_m, w_{sm}, and P_t as a function of non-dimensional mountain height for a group of runs with a=30^0.

According to Fig. 5, for the given parameters (i.e., a=30, bcosa km), the transition from DUL dominancy to LFC dominancy occurs between the nondimensional mountain height M=0.2 and 0.4. A second transition occurs approximately at M=1.1, and for higher terrain, flow reversal occurs over the windward slope and DUL contribution to the vertical motion becomes negative locally. The total precipitation starts to decrease with increasing mountain height for M>1.1, which is consistent with the previous study by Jiang (2003) using 3-D circular terrain except that the critical non-dimensional mountain height was found much larger for a 3-D circular hill (~1.32).

It should be pointed out that, the horizontal convergence term includes contributions from lateral flow confluence (i.e., dv/dy) and streamwise deceleration (i.e., du/dx). For terrain with M between 0.8 and 1.0, although, dv/dy is close to zero upstream of the vertex, du/dx is still negative, and therefore, convergence contributes to the enhancement of precipitation near the vertex. In contrast, for a straight ridge, near the center, du/dx is partially cancelled out by a positive dv/dy, and the contribution from convergence is reduced accordingly.

5. CONCLUSIONS

The dynamical funneling and precipitation associated with Moist airflow past concave-terrain is examined using a mesoscale model. The results indicate that based on the non-dimensional mountain height (M), the responses of stratified flow to convex-terrain can be dassify into three categories. For small M, the dominant contribution to the vertical motion over the windward slope comes from the direct upslope lifting (DUL). For concave-terrain with a moderate M, the

vertical motion forced by convergence of low-level airflow dominates and precipitation could be significantly enhanced by flow confluence associated with the concave-terrain. As a result, a 'wet-spot' appears over the windward slope of the concave vertex. For terrain exceeds the corresponding critical non-dimensional mountain height (i.e., 1.1 for this study), flow reversal occurs over the windward slope near the vertex. The area-integrated precipitation starts decrease with increasing mountain height and the precipitation maximum over the concave vertex disappears.

This study cautions the use of the term "funneling", which implies flow confluence. Far upstream of the terrain, the flow-level flow is always diffluent despite of terrain shapes. Confluence only occurs right upstream of the vertex of concave terrain with a small nondimensional mountain height, or with a gap near the vertex point. For terrain with a nondimensional mountain height M~1, flow is almost diffluent everywhere over the upstream side. However, compared corresponding simulations with a=0, flow diffluence along the center-streamline is significantly reduced, which contributes to the enhancement of precipitation near the vertex point.

ACKNOLWDMENT: This research is supported by the Office of Naval Research (ONR) program element 0601153N. COAMPS is a trademark of the US Naval Research Laboratory.

REFERENCE:

Bougeault, P. and Coauthors, 2001: The MAP special observing period. *Bull. Amer. Meteor. Soc.*, **82**, 433-462.

Frei C. and Schär C., 1998: A precipitation climatology of the Alps from high-resolution rain-gauge observations. *Int. J. Climatol*., **18**, 873-900.

Hodur, R. M., 1997: The Naval Research Laboratory's Coupled Ocean/Atmosphere Mesoscale Prediction System (COAMPS). *Mon. Wea. Rev*., *125*, 1414-1430.

Houze, R. A., 2001: Orographic control of precipitation: What are we learning from MAP? *Mesoscale Alpine Programme Newsl.* **14**, 3-15.

Jiang, Q., 2003: Moist dynamics and orographic precipitation. *Tellus* (A), **55**, 301-316.

Kessler, E., 1969: On the distribution and continuity of water substance in atmospheric circulations. *Meteor*. *Monog*., **10**, N32, 84pp.